

## RESEARCH ARTICLE

# 3D printing of poly(butylene adipate-co-terephthalate) (PBAT)/niobium containing bioactive glasses (BAGNb) scaffolds: Characterization of composites, in vitro bioactivity, and in vivo bone repair

Lucienne Miranda Ulbrich<sup>1</sup>  | Gabriela de Souza Balbinot<sup>2</sup>  |  
Gabriela Loewen Brotto<sup>3</sup>  | Vicente Castelo Branco Leitune<sup>2</sup>  |  
Rosane Michele Duarte Soares<sup>4</sup>  | Fabricio Mezzomo Collares<sup>2</sup>  | Deise Ponzoni<sup>1</sup> 

<sup>1</sup>Oral and Maxillofacial Surgery Unit, School of Dentistry, Universidade Federal do Rio Grande do Sul, Porto Alegre, Brazil

<sup>2</sup>Dental Materials Laboratory, School of Dentistry, Universidade Federal do Rio Grande do Sul, Porto Alegre, Brazil

<sup>3</sup>Bucomaxilofacial Surgery Department, Positivo University, Curitiba, Brazil

<sup>4</sup>Polymeric Biomaterials Laboratory (Poli-BIO), Institute of Chemistry, Universidade Federal do Rio Grande do Sul, Porto Alegre, Brazil

## Correspondence

Fabricio Mezzomo Collares, Dental Materials Laboratory, School of Dentistry, Universidade Federal do Rio Grande do Sul, Rua Ramiro Barcelos, 2492, Porto Alegre, Rio Grande do Sul, Brazil.

Email: [fabricio.collares@ufrgs.br](mailto:fabricio.collares@ufrgs.br)

## Abstract

This study aimed to produce poly(butylene adipate-co-terephthalate) (PBAT)/niobium containing bioactive glasses (BAGNb) composites scaffolds produced by fused deposition modeling (FDM) printing and evaluate their physicochemical and biological properties in vitro and in vivo. The composite filaments were produced by melt-extrusion with the addition of 10 wt% of BAGNb (PBAT/BAGNb). Filaments without BAGNb were produced as the control group (PBAT). The filaments were characterized and were used to produce 3D-printed scaffolds using FDM. The scaffolds' structure and surface properties were assessed. In vitro cell, proliferation, and cell mineralization analysis were performed. In vivo data was obtained in the rat femur model ( $n = 10$ ), and the bone repair was assessed after 15, 30, and 60 postoperative days. The printed structures presented 69.81% porosity for the PBAT/BAGNb group and 74.54% for the PBAT group. Higher cell mineralization was observed for the PBAT/BAGNb group. The in vivo data showed that the PBAT/BAGNb presented new bone formation comparable to positive controls. The combination of PBAT and BAGNb in 3D-printed scaffolds may be an alternative to produce bioactive materials with controllable shapes and properties for bone regeneration treatments.

## KEYWORDS

bone regeneration, niobium, porosity, three-dimensional printings, tissue scaffolds

## 1 | INTRODUCTION

Regenerative procedures in maxillofacial surgery commonly include the use of biomaterials to stimulate bone regeneration (Borrelli et al., 2020; Starch-Jensen et al., 2020). The use of synthetic materials in opposition to autogenous bone (AB) aims to avoid patients' morbidity and limitations in the amount of available graft for implantation (Nkenke & Neukam, 2014). Different tissue engineering approaches are used to achieve adequate bone regeneration, and scaffolds are the most commonly used devices for supporting tissue growth, vascularization, and cell activity (Balbinot et al., 2018; Bittner et al., 2019). A wide range of bone defect sizes and shapes are found, and the currently used scaffolds may not adapt adequately for surgical placement due to the material's inherent characteristics (Blume et al., 2019; Seol et al., 2014). The control of the scaffolds' macro and microscale structure is shown to modulate the formation of bone, and the control of size and shape of these materials could be achieved by an additive manufacturing process, such as fused deposition modeling (FDM; El-Rashidy et al., 2017; Marques et al., 2020).

The production of scaffolds with FDM is a well-known technique for 3D printing of materials with layer-by-layer deposition of thin filaments that allow the construction of tridimensional structures (Naghieh et al., 2016). This method allows the control of micro and macro features in the production of 3D constructs based on computer-aided modeled designs with tailored structures that are difficult to be achieved with other production methods such as porogen leaching and electrospinning (Johnson et al., 2010; Ramesh et al., 2020). Several studies have used different biocompatible and bioresorbable polymers in the FDM process (Bruyas et al., 2018). Among the possible biodegradable polymers for FDM, the poly (butylene adipate-co-terephthalate) (PBAT) has been proposed in the biomedical area due to its flexibility and easy degradation (Balbinot et al., 2021; Fukushima et al., 2013; Zehetmeyer et al., 2016). PBAT is an aliphatic-aromatic polyester that underwent low crystallization (Dou & Cai, 2016) and can be naturally degraded mainly by hydrolysis and enzymatic activity (Ren et al., 2019), leading to the release of non-toxic products (Santana-Melo et al., 2017). Due to its properties, PBAT has been studied for the development of biomedical materials, acting as support for bioactive inorganic fillers.

Niobium containing bioactive glasses (BAGNb) may be used as a source of bioactive ions to enhance the biological response in 3D-printed composite scaffolds. Bioactive glasses are well-established synthetic ceramics that can stimulate the formation of hard tissue, and tailoring these glasses' composition may increase their ability to promote bone formation. Niobium has been successfully incorporated to bioactive glasses showing the ability to enhance mineralization in vitro and in vivo (Balbinot et al., 2018, 2019, 2021). The role of niobium is not well understood, but mineral deposition and cell activation are reported and the crystalline structure is shown to be related to enhanced biological activity (Pradhan et al., 2016). Despite the advantages of these materials on bone tissue formation, the production of bioactive glass scaffolds with variable shapes and structures is considered a challenge for these materials, mainly due

to their inherent brittleness (Jones, 2015). Although the application of biomedical composites with PBAT has been studied (Fukushima et al., 2012; Santana-Melo et al., 2017) and the printability of PBAT has been described in polymeric blends (Lyu et al., 2020, 2021; Singamneni et al., 2018), the application of FDM to composites with PBAT and inorganic particles, such as the BAGNb, has not been described. This study aimed to produce PBAT/BAGNb composites scaffolds produced by FDM printing and evaluate their physico-chemical and biological properties in vitro and in vivo.

## 2 | MATERIALS AND METHOD

### 2.1 | BAGNb synthesis

Sol-gel route was used to produce the niobium containing bioactive glasses (Balbinot et al., 2018). For this synthesis, the niobium chloride ( $\text{NbCl}_5$ —CBMM Companhia Brasileira de Metalurgia e Mineração) was used as the niobium source. The formation of the silica network took place in an acidic environment with tetraethylorthosilicate (Sigma-Aldrich), triethyl phosphate (Sigma-Aldrich), calcium nitrate ( $\text{Ca}(\text{NO}_3)_2$ ; Química Moderna) and sodium nitrate ( $\text{NaNO}_3$ ; Química Moderna). The sol was aged at room temperature, and the gel was calcinated to obtain a powder. As shown in the previous report (Balbinot et al., 2018), a 45 wt%  $\text{SiO}_2$ , 24 wt%  $\text{CaO}$ , 24 wt%  $\text{Na}_2\text{O}$ , 6 wt%  $\text{P}_2\text{O}_5$ , and 1 wt%  $\text{Nb}_2\text{O}_5$  glass was obtained and sieving was performed with mesh 100 sieves. Laser diffraction analysis showed that the obtained particles presented an average particle size of 4.56  $\mu\text{m}$  with a specific surface area of 3.17  $\text{m}^2/\text{g}$  (Borrelli et al., 2020)/g, assessed via nitrogen adsorption.

### 2.2 | Composite preparation

The BAGNb particles were incorporated into the PBAT by melt extrusion. The PBAT (Ecoflex® F Blend C1200; BASF Corporation) pellets with 1.27  $\text{g}/\text{cm}^3$  at 23°C density were used. The BAGNb particles were incorporated into the PBAT at 10 wt% (PBAT/BAGNb) concentration and pure PBAT filaments were produced (PBAT). The pellets and the particles were mixed in a plastic bag immediately before the extrusion process, and the composites were prepared using twin-screw extrusion (Haake H-25, Rheomex PTW 16/25—PolyLab System). The extrusion was performed at 150 rpm rotation with a temperature profile of 120/130/130/135/140°C from the barrel section just after the feed throat to the die. The extrudate was cooled in water.

### 2.3 | Filament characterization

#### 2.3.1 | Fourier-transformed infrared spectroscopy

The chemical structure of filaments was analyzed by Fourier-transformed infrared spectroscopy (FTIR) in a spectrometer (Vertex

70—Bruker Optics) equipped with an attenuated total reflectance device (Platinum ATR-QL; Bruker Optics). The analysis was performed in the 400–4000  $\text{cm}^{-1}$  at 0.4  $\text{cm}^{-1}$  spectral resolution in 16 scans for each sample.

### 2.3.2 | Thermogravimetric analysis

PBAT and PBAT/BAGNb filaments were evaluated in a thermogravimetric analyzer (TGA Discovery—TA Instruments). All samples were weighed ( $0.5 \text{ g} \pm 0.01$ ) for the analysis. Platinum pans were used, and the range in the temperature for analysis was set between 20°C and 600°C. The heating rate was 10°C/min, and all analyses were performed under nitrogen purge (25 ml/min). The results were analyzed through the mass loss (%) after the heating process.

### 2.4 | Scaffold production

The scaffolds were produced with the composite filaments in an FDM printer (CL1, Cliever). The scaffolds were designed with a 0.5 mm distance between the deposited filaments, and the diameter of the deposited structures was 0.5 mm. The printing nozzle size was 300  $\mu\text{m}$ , and the temperature was set at 195°C. No post-production treatment was applied to the scaffolds. The scaffold design was planned in a computer-aided design software (SolidWorks—Dassault Systèmes SolidWorks Corporation). Cylindric structures measuring 500  $\mu\text{m}$  were designed creating a mesh with 500  $\mu\text{m}$  space between each other. This design was transferred to the FDM printing to obtain the scaffolds via polymer melting and deposition.

### 2.5 | Scaffolds characterization

#### 2.5.1 | Contact angle and surface-free energy

The contact angle was measured on the surface of the samples by the sessile drop method using distilled water and  $\alpha$ -bromonaphthalene. Three single drops were poured on top of the three specimens per group (6 mm diameter  $\times$  2 mm height;  $n = 3$ ) in an optical tensiometer (Theta Line, Biolin Scientific). After 10 s, the contact angle between the droplet and the material was recorded. The results were used to calculate the surface free energy of the samples according to the OWRK/Fowkes method in  $\text{mN/m}$  (Borrelli et al., 2020). Polar and dispersive components were used to calculate surface energy at the measurement software (OneAttension- Biolin Scientific), where water polar and dispersive components were 21.80 and 51.00  $\text{mN/m}$ , respectively, while the  $\alpha$ -bromonaphthalene were 0 and 44.40  $\text{mN/m}$ .

#### 2.5.2 | X-ray computed microtomography

Specimens (8 mm diameter  $\times$  2 mm height;  $n = 3$ ) were scanned using a high-resolution micro-CT system (MicroCT.SMX-90 CT; Shimadzu Corp.). The scanner was operated at 90 kV and 100 mA with 1224 resolution with a 16  $\mu\text{m}$  voxel size. The images were analyzed in ImageJ (National Institutes of Health) where the porosity, the pore size, and the connective density (connD) were assessed.

### 2.6 | Cell behavior

The preosteoblastic MC3T3-E1 cell line (Subclone-14, Banco de Células do Rio de Janeiro) was used to assess cell behavior. Cells were cultivated in alpha minimum essential medium ( $\alpha$ -Men—Thermo Fisher Scientific) supplemented with 10% fetal bovine serum (FBS—Thermo Fisher Scientific) and 1% penicillin (Thermo Fisher Scientific) and stored in a 5%  $\text{CO}_2$  at 37°C until confluency. Specimens (12 mm diameter  $\times$  2 mm height;  $n = 3$ ) were sterilized under hydrogen peroxide and immersed in culture media for 24 h at 37°C/5%  $\text{CO}_2$  to produce a conditioned medium. This medium was used to treat cells during analysis. For all tests, the culture medium without contact with materials was used as the control.

#### 2.6.1 | Cell proliferation

Sulforhodamine B (SRB) assay was used to test the influence of materials in cell proliferation. MC3T3-E1 cells were seeded at  $5 \times 10^3$  cells/well density in 96-well plates, and after 24 h, each well was treated with 100  $\mu\text{l}$  of conditioned medium for 72 h. After treatment, cells were fixed and stained (50  $\mu\text{l}$  SRB 0.4%—Sigma Aldrich). The SRB dye was quantified in a spectrophotometer (MultiskanGO, Thermo Fisher Scientific) where the absorbance at 560 nm was detected. Three specimens were used for each experiment that was performed in triplicate.

#### 2.6.2 | Cell mineralization

Alizarin S Red was used to quantify cell mineralization. An osteogenic induction media ( $\alpha$ -Men supplemented with 10% FBS, 1% Penicillin, 0.0023 g/ml  $\beta$ -glycerophosphate, and 0.05 mg/ml L-ascorbate) was used during the experiment. Cells were seeded at  $1 \times 10^4$  cells/well density in 24-well plates and treated with a conditioned medium for 7, 14, and 21 days. After each testing time, cells were fixed in formaldehyde 10% (Sigma Aldrich) and stained with 2% Alizarin S Red aqueous solution (Sigma Aldrich). Wells were imaged with a digital camera with 5 $\times$  magnification, and the obtained images were analyzed in an image software (ImageJ—National Institutes of Health). The area fraction of mineralized granules on each well was

quantified based on the red intensity threshold. The same segmentation was used for all samples. Wells treated without conditioned media were used to normalize the results in wells with treatment.

## 2.7 | In vivo

### 2.7.1 | Animals

All in vivo experiments were conducted after approval of the animal ethics committee of Universidade Positivo (registration number 411) following the Declaration of Helsinki. One hundred and twenty male rats (*Rattus norvegicus Albinus*, Wistar lineage) with an average weight of  $300 \pm 50$  g were used to perform the in vivo bone formation analysis. The animals were housed in cages under controlled room temperature ( $22 \pm 2^\circ\text{C}$ ) and humidity (40%–60%), with 12-h light/dark cycle with appropriate food and water ad libitum.

A rat femur model was used in the present study. Before the surgery, the animals were randomized in randomization software and assigned to one of the four different groups ( $n = 10$ ). Cylindric 2 mm height  $\times$  2 mm diameter PBAT/BAGNb samples were produced and sterilized in hydrogen peroxide before the implantation. Autogenous bone and deproteinized bovine bone marrow (DDBM–Bio-Oss–Geistlich) were used as positive controls. A sham surgery (SHAM) was performed with the empty bone defects to evaluate the spontaneous wound healing as a negative control.

The animals were submitted to general anesthesia and local anesthesia. The right femoral region was shaved and submitted to antiseptis and local anesthesia. A 1-cm-long incision was performed on the long axis of the femur. The femur's lateral diaphysis was exposed, and the defect was created in the femur bone with 2 mm height and 2 mm diameter with a cylindric trephine burr under constant irrigation with sterile water. The bone defects were filled according to the groups, and after the implantation, the fascia-periosteal flaps were sutured with polyglactin while for the skin, nylon was applied. The animals were observed by a veterinarian for postoperative complications after the surgery. After 15, 30, and 60 days the animals were submitted to 100% oxygen vaporized isoflurane for euthanasia. An incision was made on the area of the surgery, and the femur was sectioned and stored in 10% formalin.

### 2.7.2 | In vivo bone repair

The femoral bone samples were sectioned and analyzed by X-ray computed microtomography (MicroCT; SMX-90 CT; Shimadzu Corp.). The femur sections were analyzed with a 60 kV intensity and 100 mA with a 10  $\mu\text{m}$  voxel size in images with a 1024 resolution. An imaging software (ImageJ; National Institutes of Health) was used to quantify the new bone formation in a standardized area selected by a greyscale threshold (100–200). A region of interest was used to assess the bone density, the trabecular thickness (Tb.Th), the

trabecular separation (Tb.Sp), the trabecular number (Tb.N), the connD, and the bone fraction (BV/TV).

## 2.8 | Statistical analysis

The results of filament characterization were descriptively analyzed. The normality was assessed by Shapiro-Wilk. Student-t test was used to compare groups in the assessment of scaffold structural parameters by microCT, in the contact angle and surface free energy, in the cell proliferation analysis, and in the cell mineralization analysis at each time point. For cell mineralization between time points, one-way ANOVA was used with Tukey post hoc. Two-way ANOVA and Tukey were used to assess the differences between groups and post-operative times in the % bone area, mean density, Tb.Sp, Tb.Th, and Tb.N results. ANOVA on ranks was used for BV/TV and ConnD comparisons. All analyses were carried out with SigmaPlot 12.0 (Systat Software Inc) at 95% significance.

## 3 | RESULTS

The PBAT and PBAT/BAGNb filaments were successfully produced and presented a mean diameter of 1.75 mm, compatible with the FDM 3D printer. Fourier-transformed infrared spectroscopy spectra showed C–O and C=O vibrations at  $1150/1270\text{ cm}^{-1}$  and  $700/1700\text{ cm}^{-1}$  wavelength, respectively. Those peaks are mainly related to PBAT, while the 450 and  $1050\text{ cm}^{-1}$  absorbance are assigned to the asymmetric stretching Si–O–Si vibrations, which is related to the presence of BAGNb. The thermal degradation temperature for both materials occurred between  $350^\circ\text{C}$  and  $430^\circ\text{C}$  (Figure 1b), while the maximum degradation occurred at  $404^\circ\text{C}$ . However, due to the presence of inorganic particles, PBAT/BAGNb showed 89.84% of weight loss, while PBAT showed 96.34%. The presence of BAGNb on polymer filaments resulted in changes in the thermal degradation profile and decreased the initial degradation temperature ( $T_i = 257^\circ\text{C}$ ; Figure 1c).

The design of scaffolds is shown in Figure 2a, and representative images of printed scaffolds are shown in Figure 2b. As the presence of particle impact the printability, it can be observed that the BAGNb increases heterogeneity on the structure. The differences in the printability may be observed in the quantification of the porous structure. No statistical difference was found between groups in the porosity of produced scaffolds (PBAT: 74.54% [ $\pm 5.23$ ]; PBAT/BAGNb: 69.81% [ $\pm 8.66$ ];  $p > 0.05$ ), but reduced average pore size was found for PBAT/BAGNb (Figure 2c;  $p < 0.05$ ). Statistically significantly lower contact angle was found for PBAT/BAGNb groups (Figure 3;  $p < 0.05$ ) with water, and no statistically significant difference was found between groups ( $p > 0.05$ ) when  $\alpha$ -bromonaphtalen is used. The surface free energy was calculated using water and  $\alpha$ -bromonaphtalen, where PBAT scaffolds presented  $45.97\text{ mN/m}^2$  while PBAT/BAGNb showed  $52.73\text{ mN/m}^2$  ( $p > 0.05$ ).

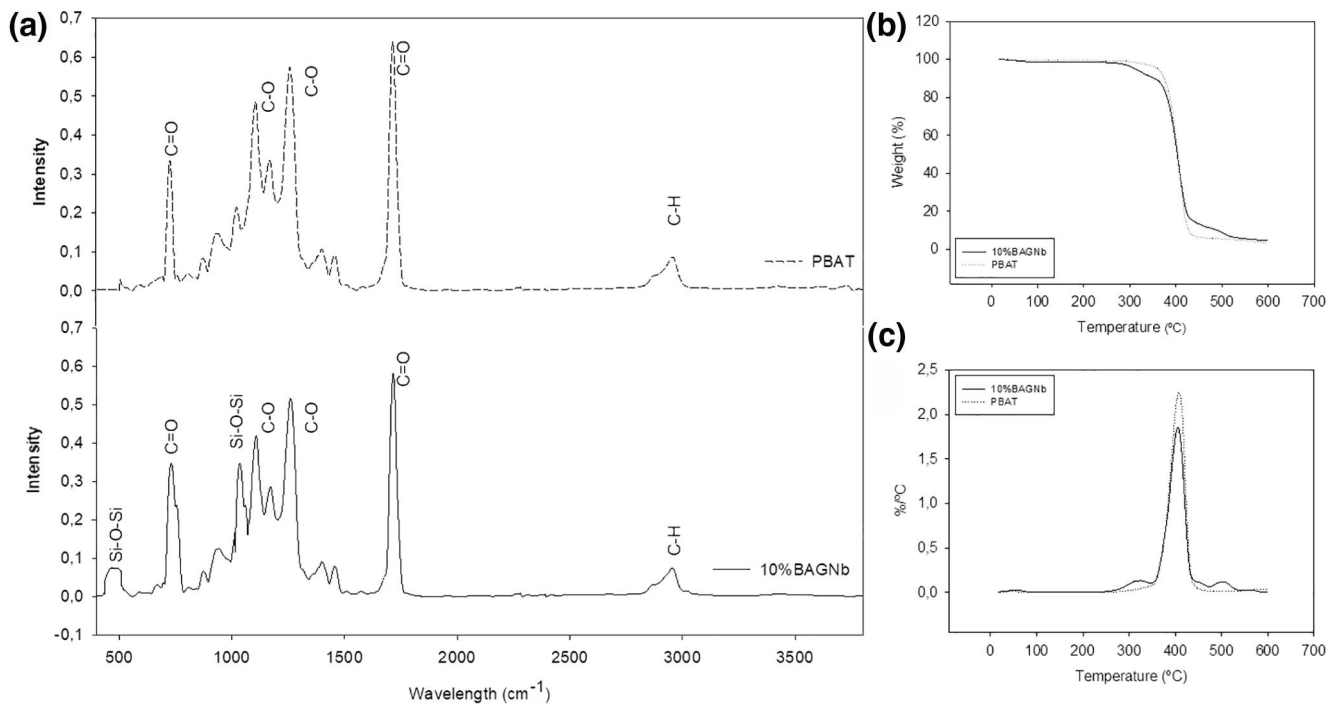


**FIGURE 1** Characterization of poly(butylene adipate-co-terephthalate) (PBAT) and PBAT/niobium containing bioactive glasses (BAGNb) filaments after the melt extrusion process. (a) Fourier-transformed infrared spectroscopy (FTIR) results for PBAT and PBAT/BAGNb materials with C-O and C=O bonding from PBAT structure and Si-O-Si bonding from BAGNb particles; (b) thermogravimetric analyzer (TGA) analysis between 20°C and 600°C with main weight loss at 350°C and 430°C. (c) % of mass loss/°C after heating between 20°C and 600°C. The mass loss for PBAT/BAGNb materials started at early temperatures with irregular increases along with the analysis

Pre-osteoblastic cell behavior was assessed through cell proliferation and cell mineralization analysis. No reduction in pre-osteoblastic cell proliferation was found in the analysis ( $p > 0.05$ ). After 14 and 21 days, increased mineralization was observed for PBAT/BAGNb when compared to the PBAT group in the mineralization assay (Figure 4). After 21 days, the area of mineralized nodules was higher than the early time points. Representative images show increased red staining in wells over time, which represents an increased formation of minerals by pre-osteoblastic cells.

In vivo bone repair is shown in Figures 5 and 6. Representative microCT reconstructions are shown in Figure 5a. On DBBM images, the presence of bovine-derived hydroxyapatite particles is observed and remained on the defect after 60 days. The wound closure for AB after 60 days was more pronounced. No increase in bone density was found between 15 and 60 days for AB and SHAM. On DBBM and PBAT/BAGNb, increased density was observed after 30 and 60 days. No statistically significant difference was found between groups and postoperative times in BV/TV and ConnD analysis. The trabecular separation was increased after 30 and 60 days for AB, SHAM, and PBAT/BAGNb groups ( $p > 0.05$ ). The trabecular thickness (Tb.Th) parameter was increased over time for the PBAT/BAGNb ( $p < 0.05$ ). Although the thicker trabecular structure was formed, the trabecular number (Tb.N) was reduced over time in this group.

## 4 | DISCUSSION

3D-printed scaffolds have been studied as an alternative to regenerative treatments, and maxillofacial regenerative therapies may benefit from the development of custom-built scaffolds with bioactive properties (Abar et al., 2020; Korn et al., 2020; Lopez et al., 2018; Mehra et al., 2011). In the present study, PBAT and BAGNb particles were used to produce melt-extruded filaments that were used for FDM 3D printing of scaffolds. The PBAT/BAGNb printed scaffolds presented increased wettability and increased the ability to promote cell mineralization. In vivo analysis showed bone formation for PBAT/BAGNb scaffolds with comparable results to the AB and deproteinized bone bovine marrow.

To allow the 3D printing of PBAT/BAGNb composites, the polymer processing via melt-extrusion was applied as the melting of PBAT leads to the easier spreading of particles into the polymer and allows the conformation of produced composites into filaments to be used for scaffold manufacturing (Zagho et al., 2018). Although the chosen parameter for extrusion was selected based on the chemical structure of PBAT, this process can be responsible for changes in the polymer structure, which was not the goal in the material processing. The parameters of extrusion were optimized for the composites using temperatures that are known to be effective for PBAT processing (Zehetmeyer et al., 2016). The 10 wt% BAGNb concentration was selected during this process to allow the printability of extruded

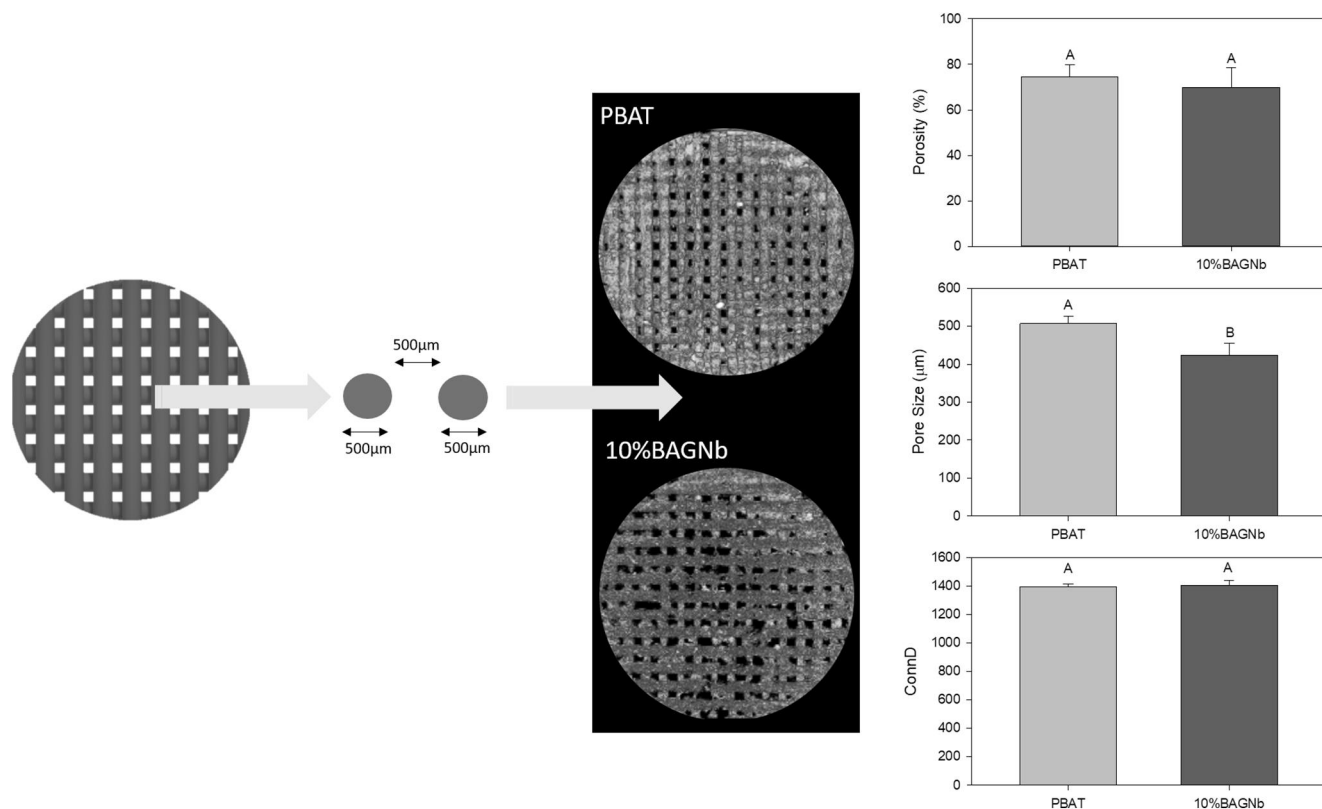


**FIGURE 2** Design of produced scaffolds and structural characteristics. (a) The design proposed for the scaffolds to be produced by fused deposition modeling (FDM) printing. (b) 3D reconstruction of microCT imaged poly(butylene adipate-co-terephthalate) (PBAT) and PBAT/niobium containing bioactive glasses (BAGNb) scaffolds. (c) Porosity, pore size, and connective density (connD) of PBAT and PBAT/BAGNb scaffolds

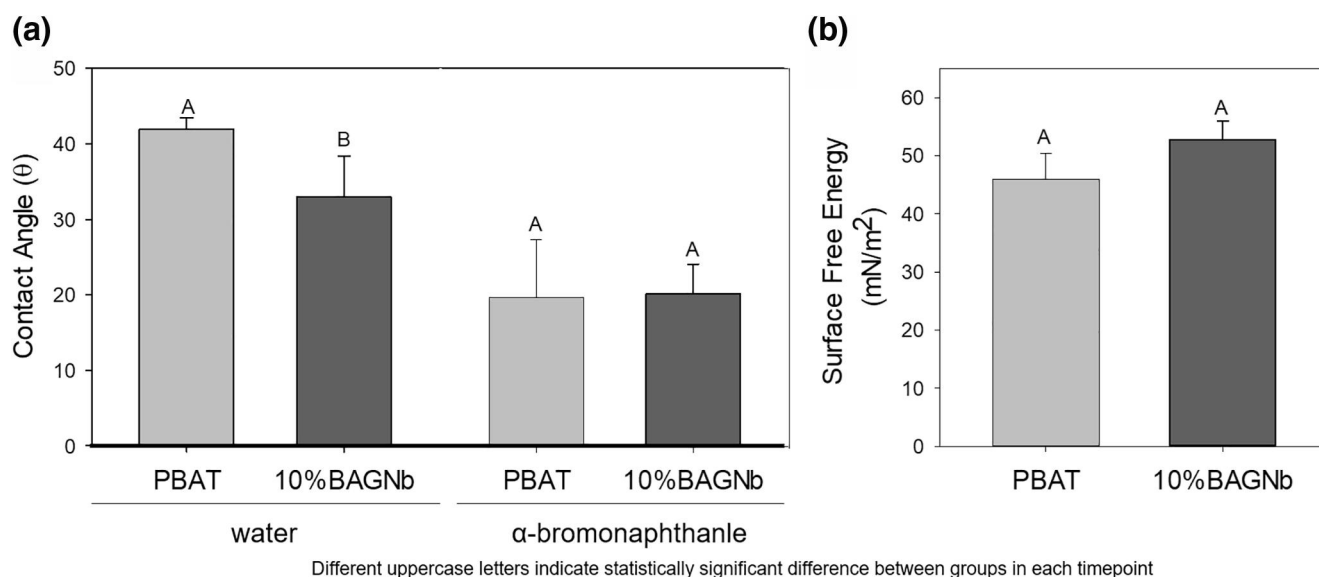


**FIGURE 3** Surface wettability of developed scaffolds. (a) Water and α-bromonaphthalene contact angle on the surface of poly(butylene adipate-co-terephthalate) (PBAT) and PBAT/niobium containing bioactive glasses (BAGNb) scaffolds. (b) Surface-free energy (mN/m<sup>2</sup>) is calculated based on the contact angle of polar and non-polar liquids on the surface of scaffolds

filaments by the FDM nozzle. The addition of BAGNb is observed by the presence of Si-O-Si bonding on FTIR (Figure 1a), and the influence of particles on thermal behavior was also observed. The weight

loss takes place in lower temperatures for the PBAT/BAGNb filaments (Figure 1b and 1c). This may be related to a modification in the polymeric structure and crystallinity by the dispersion of inorganic

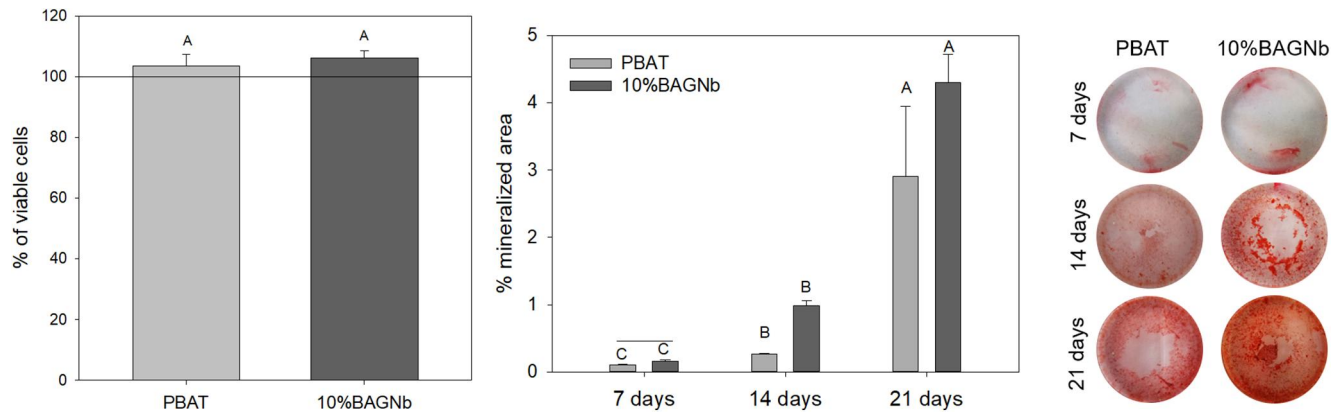


FIGURE 4 Pre-osteoblastic cell behavior analysis for poly(butylene adipate-co-terephthalate) (PBAT) and PBAT/niobium containing bioactive glasses (BAGNb) scaffolds. (a) Cell proliferation results (%) after 72 h of treatment with material's conditioned medium and staining with sulforhodamine B (SRB). (b) Quantitative analysis of % of the mineralized area after 7, 14, and 21 days and (c) representative images of Alizarin S red analysis after 7, 14, and 21 days of culture

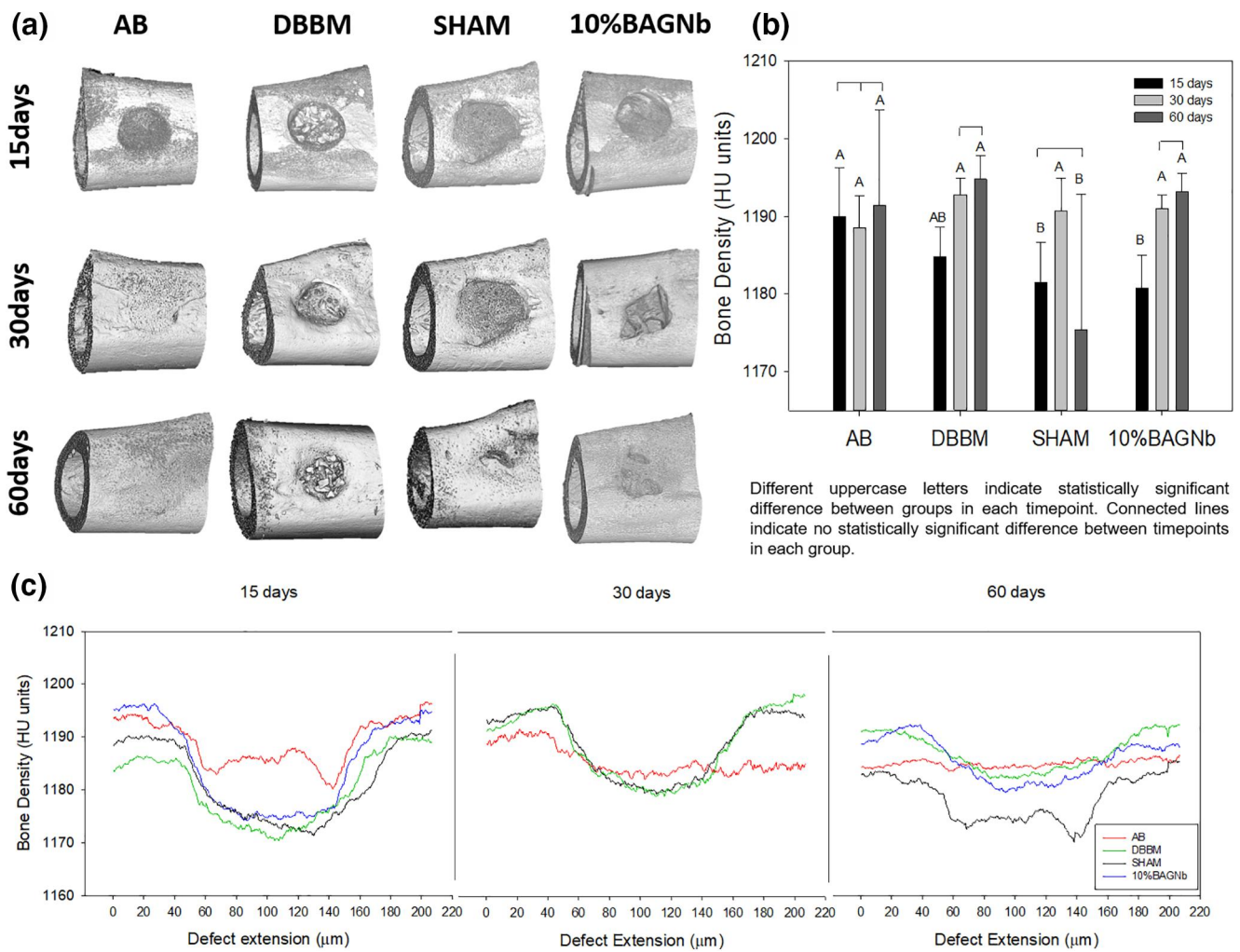
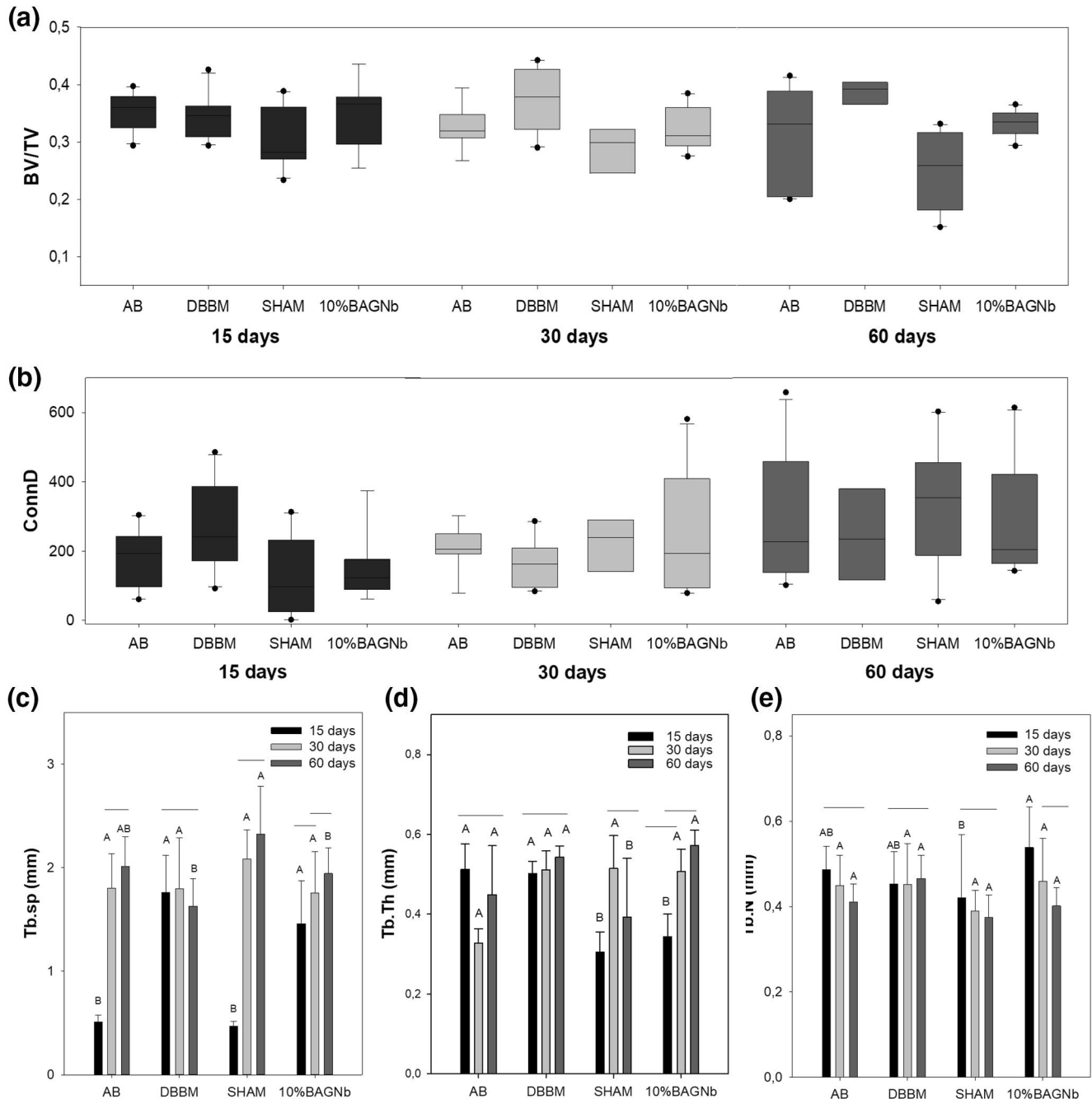


FIGURE 5 (a) Representative images of bone after 15, 30, and 60 days with different treatments. (b) Bone density through the defect extension after different postoperative times. (c) Bone density in pixel density after different treatments

particles in between the chains that may modify the breaking of ester bonds in PBAT, which are known to be responsible for the polymer degradation (Fukushima et al., 2013).

The PBAT and the BAGNb were used in the present study as bioresorbable materials in a well-designed tridimensional structure that aims to promote better interaction between material and



Different uppercase letters indicate statistically significant difference between groups in each timepoint. Connected lines indicate no statistically significant difference between timepoints in each group.

**FIGURE 6** Morphometric analysis of in vivo bone repair. (a) BV/TV and (b) connective density (connD) values for different groups over time. The trabecular structure of bone after different treatments in each postoperative time was shown in (c), where the Tb.Th, Tb.Sp, and Tb.N values were analyzed for the analysis of bone quality during wound healing

surrounding tissues (Metz et al., 2019). The 3D printing was possible as the concentration of BAGNb was optimized, and by using 10 wt%, a good resolution was found. The presence of particles may impair the adequate deposition of layers during the fused deposition, leading to differences in printed structures' resolution, and this may be related to the pore size results found for PBAT/BAGNb. The porosity and pore size values of PBAT/BAGNb follow the findings of similar materials (Bruyas et al., 2018; Buj-Corral et al., 2018). They may be

related to an increased surface area for ion release that could promote increased cell activity, as observed in Figure 4. The values were within the optimal pore size for bone growth, showing to promote higher deposition of bone due to increased interaction in the material/tissue interface (Hassan et al., 2019). This may be related to bone formation over the defect, where this interaction could result in a homogeneous formation from the defect limits to the center (Figure 5b and 5c).

Surface properties may increase the interaction between scaffolds and cells. It is well-known that most of the bioresorbable synthetic polymers used for composite bone regeneration scaffolds are hydrophobic (Shkarina et al., 2018; Vaikkath et al., 2016). The water contact angle values for PBAT and PBAT/BAGNb groups are lower when compared to PLLA (Cairns et al., 2012), PLGA (Arabpour et al., 2019), and PCL (Shkarina et al., 2018), that present contact angle values between 100° and 120°. The bioactive glass particles are highly hydrophilic, and the presence of 10 wt% BAGNb into the composites reduced the contact angle significantly. The macro- and micro-scale structures also play an important role in the wetting properties of materials, and an increase in the surface roughness promoted by the particles could modify the wetting response on these materials. Increasing the wettability in implanted materials by reducing the contact angle, as observed in this study, may lead to better interaction between the cell and tissue environment. Enhanced cell adhesion is found for hydrophilic scaffolds as physiological fluids could easily interact with materials mediating their addition by extracellular matrix receptors leading to integrin binding (Fan & Guo, 2020). Once cell adherence takes place the cell metabolism may be modulated promoting proliferations, spreading and differentiation over the scaffold. Besides bone formation, the facilitated adhesion of clastic cells that are related to cell/enzyme mediated degradation and the enhanced hydrolysis promoted by the hydrophilic nature of scaffolds may contribute to its degradation over time (Ren et al., 2019). Although *in vivo* degradation involves the activity of osteoclastic cells and is mediated by cell-to-cell communication during the bone remodeling process, the degradation of the ester linkages in PBAT is water-induced (Scaffaro et al., 2019), and thus, increasing the wettability may fasten the polymer and ion dissolution in bone defects.

PBAT presents reduced thermal stability (Mohanty & Nayak, 2012), and previous studies (dos Santos Silva et al., 2019; Santana-Melo et al., 2017) have shown the degradation of PBAT *in vivo*, which, according to the results of this study, could be accelerated by the incorporation of BAGNb particles into the PBAT polymeric network (Figure 1b). The degradation of PBAT/BAGNb materials is related to the degradation of polymeric chains and the solubility of bioactive ions from BAGNb particles. Bioactive ions are leached immediately after the contact to aqueous solutions (Balbinot et al., 2018; Hoppe et al., 2011), and further degradation may contribute to releasing particles that are entrapped into the polymeric structure of PBAT. In this study, an indirect analysis was conducted, and although the absence of contact between the materials and cells is a limitation, this analysis aimed to understand the effect of released products on cell behavior. Few studies reported the biocompatibility of PBAT (dos Santos Silva et al., 2019; Fukushima et al., 2013; Santana-Melo et al., 2017), which is supported by the findings of the present study where no reduction in cell viability was observed for PBAT and PBAT/BAGNb scaffolds treatment in pre-osteoblastic cell behavior. The effect of BAGNb on pre-osteoblastic cell mineralization was reported before (Balbinot et al., 2018), and the ability of these cells to produce mineralized structures is related

to their differentiation into osteoblasts (Czekanska et al., 2012). The ability to modify cell response is related to cell recruiting *in vivo* and to the differentiation of mesenchymal stem cells into osteogenic lineages that present the machinery to deposit osteogenic matrix.

The PBAT/BAGNb scaffolds were used considering the *in vitro* characterization and the cell behavior analysis. Rat animal models were used in this analysis to provide a feasible overview of the activity of developed materials and their safety. No postoperative complications were observed for the PBAT/BAGNb treated animals, and no sign of local or systemic toxicity was observed, corroborating with previous reports that showed PBAT as a safe material for biomedical applications (dos Santos Silva et al., 2019; Santana-Melo et al., 2017). Autogenous bone was used as a control as it is considered the gold standard for bone regeneration procedures, while DBBM is shown to produce increased bone volume in regenerative procedures (Papageorgiou et al., 2016). The high patient morbidity associated with the AB (Pereira et al., 2019) and the lack of structural organization and the lower solubility (Kuchler et al., 2019) of DBBM are the main drawbacks of those treatments that may be overcome by the developed materials. After 15, 30, and 60 days of follow up PBAT/BAGNb results were comparable to the controls considering the density along with the defect (Figure 5a and 5c). These results show that PBAT/BAGNb materials supported mineralized tissue formation along with the defect on the femur model in rats. A homogeneous bone formation was found along with the defect in the same pattern observed for the positive controls (Figure 5c).

PBAT/BAGNb scaffolds presented increasingly trabecular thickness (Tb.Th) over time (Figure 6c), and these results may indicate the organization of formed bone over time with comparable parameters found for AB and DBBM. These parameters indicate bone maturation from the early bone formation at 15 days until 60 days of wound healing. The formation of bone tissue and the ability to bone remodeling after bone regeneration procedures are required features of bone regeneration treatments, and materials should allow this physiological effect of bone maturation. In this study, BAGNb particles were used to stimulate bone formation, which has been shown previously in similar animal models (Balbinot et al., 2019). Even in low particle concentration (10 wt%), bone formation was increased, and the formed bone was able to be modified over time, indicating their maturation (Figure 6c). This behavior was not observed on DBBM granules as no significant difference was found in this parameter over time, probably due to the highly crystalline hydroxyapatite particles that are less prone to degradation (Kuchler et al., 2019) while BAGNb particles are highly soluble and may present increased interaction with tissues. The adequate bone formation induced in this initial non-critical model in the femur shows the potential of these materials to be used in the further analysis for regenerative bone procedures where custom-build structure may be produced allowing the adaptation of implants in surgical site for personalized procedures.

The production of composite scaffolds through additive manufacturing is established as an alternative for the design of controlled structures for tissue-engineered treatments, and the

development of bioactive materials for this application is essential for the increase in the understanding of the biomedical application of 3D printing. The production of personalized materials to match the shape and size of bone defects could be translated into materials that facilitate regenerative treatments. This study's results are the first that showed the printability of PBAT composites and their safety and bioactivity with the addition of BAGNb particles. The control of scaffold structure and the ability to produce these materials in tailored shapes for bone regeneration purposes enlighten the developed scaffolds' potential to be applied to tissue engineering approaches.

## 5 | CONCLUSION

The PBAT/BAGNb composites were successfully produced and used for 3D printing of bone regeneration scaffolds. The developed scaffolds contributed to osteogenic activity in vitro and in vivo, showing that the combination between PBAT and BAGNb in 3D-printed scaffolds may be an alternative for producing bioactive materials with controllable shapes and properties for bone tissue engineering.

## ACKNOWLEDGMENTS

Gabriela de Souza Balbinot would like to thank CAPES "Coordenação de Aperfeiçoamento de Pessoal de Nível Superior—Brasil—Finance Code 001." The authors gratefully acknowledge the CBMM (Companhia Brasileira de Metalurgia e Mineração) for providing the Niobium Chloride used in this study.

## CONFLICT OF INTEREST

The authors declare that they have no known competing financial interests or personal relationships that could have appeared to influence the work reported in this paper.

## AUTHOR CONTRIBUTIONS

**Lucienne Miranda Ulbrich:** Investigation, Formal Analysis, Data curation, Project Administration. **Gabriela de Souza Balbinot:** Conceptualization, Investigation, Formal Analysis, Data curation, Writing - Original Draft. **Gabriela Loewen Brotto:** Investigation. **Vicente Castelo Branco Leitune:** Conceptualization, Methodology, Writing - Review & Editing, Founding Acquisition. **Rosane Michele Duarte Soares:** Methodology, Writing - Review & Editing, Founding Acquisition. **Fabricio Mezzomo Collares:** Conceptualization, Methodology, Writing - Review & Editing, Founding Acquisition. **Deise Ponzoni:** Writing - Review & Editing, Supervision.

## DATA AVAILABILITY STATEMENT

The data that support the findings of this study are available from the corresponding author upon reasonable request.

## ORCID

Lucienne Miranda Ulbrich  <https://orcid.org/0000-0002-1503-1163>  
Gabriela de Souza Balbinot  <https://orcid.org/0000-0001-9076-2460>

Gabriela Loewen Brotto  <https://orcid.org/0000-0002-0141-2547>

Vicente Castelo Branco Leitune  <https://orcid.org/0000-0002-5415-1731>

Rosane Michele Duarte Soares  <https://orcid.org/0000-0002-5225-7559>

Fabricio Mezzomo Collares  <https://orcid.org/0000-0002-1382-0150>

Deise Ponzoni  <https://orcid.org/0000-0003-2855-7495>

## REFERENCES

- Abar, B., Alonso-Calleja, A., Kelly, A., Kelly, C., Gall, K., & West, J. L. (2020). 3D printing of high-strength, porous, elastomeric structures to promote tissue integration of implants. *Journal of Biomedical Materials Research Part A*, 109(1), 54–63. [cited 2020 November 13]; Available from: <https://onlinelibrary-wiley.ez45.periodicos.capes.gov.br/doi/full/10.1002/jbm.a.37006>
- Arabpour, Z., Baradaran-Rafi, A., Bakhshaiesh, N. L., Ai, J., Ebrahimi-Barough, S., Esmaeili Malekabadi, H., Nazeri, N., Vaez, A., Salehi, M., Sefat, F., & Ostad, S. N. (2019). Design and characterization of biodegradable multi layered electrospun nanofibers for corneal tissue engineering applications. *Journal of Biomedical Materials Research Part A*, 107(10), 2340–2349.
- Balbinot, G. de S., Bahlis, E. A. da C., Visioli, F., Leitune, V. C. B., Soares, R. M. D., & Collares, F. M. (2021). Polybutylene-adipate-terephthalate and niobium-containing bioactive glasses composites: Development of barrier membranes with adjusted properties for guided bone regeneration. *Materials Science and Engineering. C, Materials for Biological Applications*, 125, 112115.
- Balbinot, G. de S., Collares, F. M., Visioli, F., Soares, P. B. F., Takimi, A. S., Samuel, S. M. W., & Leitune, V. C. B. (2018). Niobium addition to sol-gel derived bioactive glass powders and scaffolds: In vitro characterization and effect on pre-osteoblastic cell behavior. *Dental Materials*, 34(10), 1449–1458.
- Balbinot, G. de S., Leitune, V. C. B., Ponzoni, D., & Collares, F. M. (2019). Bone healing with niobium-containing bioactive glass composition in rat femur model: A micro-CT study. *Dental Materials*, 35(10), 1490–1497.
- Bittner, S. M., Smith, B. T., Diaz-Gomez, L., Hudgins, C. D., Melchiorri, A. J., Scott, D. W., Fisher, J. P., & Mikos, A. G. (2019). Fabrication and mechanical characterization of 3D printed vertical uniform and gradient scaffolds for bone and osteochondral tissue engineering. *Acta Biomaterialia*, 90, 37–48.
- Blume, O., Back, M., Born, T., & Donkiewicz, P. (2019). Reconstruction of a unilateral alveolar cleft using a customized allogenic bone block and subsequent dental implant placement in an adult patient. *Journal of Oral and Maxillofacial Surgery*, 77(10), 2127.e1–2127.e11.
- Borrelli, M. R., Hu, M. S., Longaker, M. T., & Lorenz, H. P. (2020). Tissue engineering and regenerative medicine in craniofacial reconstruction and facial aesthetics. *Journal of Craniofacial Surgery*, 31(1), 15–27.
- Bruyas, A., Lou, F., Stahl, A. M., Gardner, M., Maloney, W., Goodman, S., & Yang, Y. P. (2018). Systematic characterization of 3D-printed PCL/ $\beta$ -TCP scaffolds for biomedical devices and bone tissue engineering: Influence of composition and porosity. *Journal of Materials Research*, 33(14), 1948–1959.
- Buj-Corral, I., Bagheri, A., & Petit-Rojo, O. (2018). 3D printing of porous scaffolds with controlled porosity and pore size values. *Materials (Basel)*, 11(9).
- Cairns, M.-L., Dickson, G. R., Orr, J. F., Farrar, D., Hardacre, C., Sa, J., Lemoine, P., Mughal, M. Z., & Buchanan, F. J. (2012). The potential of electron beam radiation for simultaneous surface modification and bioresorption control of PLLA. *Journal of Biomedical Materials Research Part A*, 100(9), 2223–2229.
- Czekanska, E. M., Stoddart, M. J., Richards, R. G., & Hayes, J. S. (2012). In search of an osteoblast cell model for in vitro research. *European Cells and Materials*, 24, 1–17.

- dos Santos Silva, A., Rodrigues, B. V. M., Oliveira, F. C., Carvalho, J. O., de Vasconcellos, L. M. R., de Araújo, J. C. R., Marciano, F. R., & Lobo, A. O. (2019). Characterization and in vitro and in vivo assessment of poly(butylene adipate-co-terephthalate)/nano-hydroxyapatite composites as scaffolds for bone tissue engineering. *Journal of Polymer Research*, 26(2), 53.
- Dou, Q., & Cai, J. (2016). Investigation on polylactide (PLA)/poly(butylene adipate-co-terephthalate) (PBAT)/bark flour of plane tree (PF) eco-composites. *Materials (Basel)*, 9(5).
- El-Rashidy, A. A., Roether, J. A., Harhaus, L., Kneser, U., & Boccaccini, A. R. (2017). Regenerating bone with bioactive glass scaffolds: A review of in vivo studies in bone defect models. *Acta Biomaterialia*, 62, 1–28.
- Fan, H., & Guo, Z. (2020). Bioinspired surfaces with wettability: Biomolecule adhesion behaviors. *Biomaterials Science*, 8(6), 1502–1535.
- Fukushima, K., Rasyida, A., & Yang, M.-C. (2013). Characterization, degradation and biocompatibility of PBAT based nanocomposites. *Applied Clay Science*, 80–81, 291–298.
- Fukushima, K., Wu, M.-H., Bocchini, S., Rasyida, A., & Yang, M.-C. (2012). PBAT based nanocomposites for medical and industrial applications. *Materials Science and Engineering. C, Materials for Biological Applications*, 32(6), 1331–1351.
- Hassan, M. N., Yassin, M. A., Suliman, S., Lie, S. A., Gjengedal, H., & Mustafa, K. (2019). The bone regeneration capacity of 3D-printed templates in calvarial defect models: A systematic review and meta-analysis. *Acta Biomaterialia*, 91, 1–23.
- Hoppe, A., Güldal, N. S., & Boccaccini, A. R. (2011). A review of the biological response to ionic dissolution products from bioactive glasses and glass-ceramics. *Biomaterials*, 32(11), 2757–2774.
- Johnson, T., Bahrampourian, R., Patel, A., & Mequanint, K. (2010). Fabrication of highly porous tissue-engineering scaffolds using selective spherical porogens. *Bio-Medical Materials and Engineering*, 20(2), 107–118.
- Jones, J. R. (2015). Reprint of: Review of bioactive glass: From Hench to hybrids. *Acta Biomaterialia*, 23(Supplement), S53–S82.
- Korn, P., Ahlfeld, T., Lahmeyer, F., Kilian, D., Sembdner, P., Stelzer, R., Pradel, W., Franke, A., Rauner, M., Range, U., & Stadlinger, B. (2020). 3D printing of bone grafts for cleft alveolar osteoplasty—in vivo evaluation in a preclinical model. *Frontiers in Bioengineering and Biotechnology*, 88, 217. [cited 2020 May 18]; Available from: <https://www.ncbi.nlm.nih.gov/pmc/articles/PMC7109264/>
- Kuchler, U., Dos Santos, G. M., Heimel, P., Stähli, A., Strauss, F. J., Tangl, S., & Gruber, R. (2019). DBBM shows no signs of resorption under inflammatory conditions. An experimental study in the mouse calvaria. *Clinical Oral Implants Research*, 31(1), 10–17.
- Lopez, C. D., Witek, L., Torroni, A., Flores, R. L., Demissie, D. B., Young, S., Cronstein, B. N., & Coelho, P. G. (2018). The role of 3D-printing in treating craniomaxillofacial congenital anomalies. *Birth Defects Research*, 110(13), 1055–1064.
- Lyu, Y., Chen, Y., Lin, Z., Zhang, J., & Shi, X. (2020). Manipulating phase structure of biodegradable PLA/PBAT system: Effects on dynamic rheological responses and 3D printing. *Composites Science and Technology*, 200, 108399.
- Lyu, Y., Zhao, H., Wen, X., Lin, L., Schlarb, A. K., & Shi, X. (2021). Optimization of 3D printing parameters for high-performance biodegradable materials. *Journal of Applied Polymer Science*, 138(32), 50782.
- Marques, A., Miranda, G., Silva, F., Pinto, P., & Carvalho, Ó. (2020). Review on current limits and potentialities of technologies for biomedical ceramic scaffolds production. *Journal of Biomedical Materials Research Part B: Applied Biomaterials*, 109(3), 377–393. [cited 2020 November 13]; Available from: <https://onlinelibrary-wiley.ez45.periodicos.capes.gov.br/doi/10.1002/jbm.b.34706>
- Mehra, P., Miner, J., D'Innocenzo, R., & Nadershah, M. (2011). Use of 3-D stereolithographic models in oral and maxillofacial surgery. *Journal of Oral and Maxillofacial Surgery*, 10(1), 6–13.
- Metz, C., Duda, G. N., & Checa, S. (2019). Towards multi-dynamic mechano-biological optimization of 3D-printed scaffolds to foster bone regeneration. *Acta Biomaterialia*, 101, 117–127.
- Mohanty, S., & Nayak, S. K. (2012). Biodegradable nanocomposites of poly(butylene adipate-co-terephthalate) (PBAT) and organically modified layered silicates. *Journal of Polymers and the Environment*, 20(1), 195–207.
- Naghieh, S., Karamooz Ravari, M. R., Badrossamay, M., Foroomezeh, E., & Kadkhodaei, M. (2016). Numerical investigation of the mechanical properties of the additive manufactured bone scaffolds fabricated by FDM: The effect of layer penetration and post-heating. *Journal of the Mechanical Behavior of Biomedical Materials*, 59, 241–250.
- Nkenke, E., & Neukam, F. W. (2014). Autogenous bone harvesting and grafting in advanced jaw resorption: Morbidity, resorption and implant survival. *European Journal of Oral Implantology*, 7(Suppl 2), S203–S217.
- Papageorgiou, S. N., Papageorgiou, P. N., Deschner, J., & Götz, W. (2016). Comparative effectiveness of natural and synthetic bone grafts in oral and maxillofacial surgery prior to insertion of dental implants: Systematic review and network meta-analysis of parallel and cluster randomized controlled trials. *Journal of Dentistry*, 48, 1–8.
- Pereira, R. S., Pavelski, M. D., Griza, G. L., Boos, F. B. J. D., & Hochuli-Vieira, E. (2019). Prospective evaluation of morbidity in patients who underwent autogenous bone-graft harvesting from the mandibular symphysis and retromolar regions. *Clinical Implant Dentistry and Related Research*, 21(4), 753–757.
- Pradhan, D., Wren, A. W., Misture, S. T., & Mellott, N. P. (2016). Investigating the structure and biocompatibility of niobium and titanium oxides as coatings for orthopedic metallic implants. *Materials Science and Engineering. C, Materials for Biological Applications*, 58, 918–926.
- Ramesh, B., Cherian, K. M., & Fakoya, A. O. J. (2020). Fabrication and electrospinning of 3D biodegradable poly-L-lactic acid (PLLA) nanofibers for clinical application. *Methods in Molecular Biology*, 2125, 119–128.
- Ren, Y., Hu, J., Yang, M., & Weng, Y. (2019). Biodegradation behavior of poly (lactic acid) (PLA), poly (butylene adipate-co-terephthalate) (PBAT), and their blends under digested sludge conditions. *Journal of Polymers and the Environment*, 27(12), 2784–2792.
- Santana-Melo, G. F., Rodrigues, B. V. M., da Silva, E., Ricci, R., Marciano, F. R., Webster, T. J., Vasconcellos, L. M. R., & Lobo, A. O. (2017). Electrospun ultrathin PBAT/nHAP fibers influenced the in vitro and in vivo osteogenesis and improved the mechanical properties of neofomed bone. *Colloids and Surfaces B: Biointerfaces*, 155, 544–552.
- Scaffaro, R., Maio, A., Suter, F., Gulino, E. F., & Morreale, M. (2019). Degradation and recycling of films based on biodegradable polymers: A short review. *Polymers (Basel)*, 11(4). [cited 2020 November 2]; Available from: <https://www.ncbi.nlm.nih.gov/pmc/articles/PMC6523205/>
- Seol, Y.-J., Park, J. Y., Jung, J. W., Jang, J., Girdhari, R., Kim, S. W., & Cho, D. W. (2014). Improvement of bone regeneration capability of ceramic scaffolds by accelerated release of their calcium ions. *Tissue Engineering Part A*, 20(21–22), 2840–2849.
- Shkarina, S., Shkarin, R., Weinhardt, V., Melnik, E., Vacun, G., Kluger, P., Loza, K., Epple, M., Ivlev, S. I., Baumbach, T., & Surmeneva, M. A. (2018). 3D biodegradable scaffolds of polycaprolactone with silicate-containing hydroxyapatite microparticles for bone tissue engineering: High-resolution tomography and in vitro study. *Scientific Reports*, 8(1), 1–3. [cited 2018 August 4]; Available from: <https://www.ncbi.nlm.nih.gov/pmc/articles/PMC5995873/>
- Singamneni, S., Smith, D., LeGuen, M.-J., & Truong, D. (2018). Extrusion 3D printing of polybutyrate-adipate-terephthalate-polymer composites in the pellet form. *Polymers (Basel)*, 10(8). [cited 2019 November 27]; Available from: <https://www.ncbi.nlm.nih.gov/pmc/articles/PMC6403630/>

- Starch-Jensen, T., Deluiz, D., & Tinoco, E. M. B. (2020). Horizontal alveolar ridge augmentation with allogeneic bone block graft compared with autogenous bone block graft: A systematic review. *Journal of Oral & Maxillofacial Research*, 11(1). [cited 2020 May 18]; Available from: <https://www.ncbi.nlm.nih.gov/pmc/articles/PMC7191383/>
- Vaikkath, D., Anitha, R., Sumathy, B., & Nair, P. D. (2016). A simple and effective method for making multipotent/multilineage scaffolds with hydrophilic nature without any postmodification/treatment. *Colloids and Surfaces B: Biointerfaces*, 141, 112–119.
- Zagho, M. M., Hussein, E. A., & Elzatahry, A. A. (2018). Recent overviews in functional polymer composites for biomedical applications. *Polymers (Basel)*, 10(7).
- Zehetmeyer, G., Meira, S. M. M., Scheibel, J. M., Oliveira, R. V. B. de, Brandelli, A., & Soares, R. M. D. (2016). Influence of melt processing on biodegradable nisin-PBAT films intended for active food packaging applications. *Journal of Applied Polymer Science*, 133(13). [cited

2020 Oct 15]; Available from: <https://onlinelibrary.wiley.com/doi/abs/10.1002/app.43212>

**How to cite this article:** Ulbrich, L. M., Balbinot, G. d. S., Brotto, G. L., Leitune, V. C. B., Soares, R. M. D., Collares, F. M., & Ponzoni, D. (2021). 3D printing of poly(butylene adipate-co-terephthalate) (PBAT)/niobium containing bioactive glasses (BAGNb) scaffolds: Characterization of composites, in vitro bioactivity, and in vivo bone repair. *Journal of Tissue Engineering and Regenerative Medicine*, 1–12. <https://doi.org/10.1002/term.3276>